Hindawi
Advances in Civil Engineering
Volume 2019, Article ID 4324528, 20 pages
https://doi.org/10.1155/2019/4324528

Research Article

Experimental Study on Bearing Capacity of Reinforced Steel Tubular Scaffold under Uniform Loads

Li Jia,[1] Hongbo Liu,[2] Zhihua Chen,[2] Yang Liu,[3] and Yapeng Wu[3]

[1]*Architectural Design and Research Institute of Tianjin University, Tianjin 300072, China*
[2]*State Key Laboratory of Hydraulic Engineering Simulation and Safety, Tianjin University, Tianjin 300072, China*
[3]*School of Civil Engineering, Tianjin University, Tianjin 300072, China*

Correspondence should be addressed to Hongbo Liu; hbliu@tju.edu.cn

Received 26 April 2019; Revised 27 July 2019; Accepted 14 August 2019; Published 29 September 2019

Academic Editor: Melina Bosco

Copyright © 2019 Li Jia et al. This is an open access article distributed under the Creative Commons Attribution License, which permits unrestricted use, distribution, and reproduction in any medium, provided the original work is properly cited.

Five groups of tests were designed to analyze the influence of node types (fastener connection and mortise-and-tenon joint) and reinforcement modes of top horizontal cross rods (weak truss and stiffening truss) on the bearing capacity of the steel tubular scaffold under vertical uniform loads. Loading phenomenon, bearing capacity, failure mode, displacement at key positions, and strain development characteristics during tests were analyzed. The following conclusions were drawn: (1) The fastener scaffold reinforced by a top truss showed the highest bearing capacity and high material utilization. (2) The fastener scaffold reinforced by a top weak truss increased the bearing capacity and caused coordinated deformation of the top horizontal force rods. (3) The node displacement of the mortise-and-tenon scaffold was smaller than that of the fastener joint, whereas its bearing capacity was higher. (4) Vertical diagonal bracing can slightly increase the bearing capacity of the mortise-and-tenon scaffold but can also constrain the deformation of the vertical rods and change the failure mode.

1. Introduction

As temporary support structures, scaffolds have been widely applied in engineering construction. At present, common scaffold systems can be divided into fastener, door-type, cuplock-type, access scaffold, and inserting-type steel tubular scaffolds, as shown in Figure 1. The temporary application of scaffolds has led to few studies on its structural performance and design method. Nevertheless, frequent and recent collapse and accidents of scaffolds due to improper site management and unreasonable design have resulted in serious economic loss and casualties. Therefore, research on structural performance and design method of scaffolds has attracted increasing attention from engineering and academic circles.

The scaffold is a temporary structure, but its mechanical properties are more complicated than those of permanent steel structures. This is attributed to many factors, such as structural defects caused by complicated joint performance, flexible and changeable site installation, repeated use of components, and complicated damage distribution. Chan et al. [1], Peng et al. [2–6], Weesner and Jones [7], and Yu et al. [8] conducted theoretical and experimental studies on the stability capacity and design method of door-type scaffolds. Pienko and Blazik-Borowa [9] determined the capacity of the key joint in the inserting-type scaffold based on numerical analysis. The study likewise considered nonlinear materials and the interaction between particular joint elements. Peng et al. [10] investigated the load capacities and failure modes of the inserting-type scaffold based on experimental tests supplemented by analyses. Zhang et al. [11–13] studied the cuplock-type scaffold by using the probability-based design method. Godley and Beale [14–16], Yue et al. [17], Ao and Li [18], and Liu et al. [19, 20] conducted systematic studies on stability capacity and design method of structural steel tubes and coupler scaffolds. Cimellaro and Domaneschi [21] comprehensively performed finite element simulations considering the imperfections on three types of steel scaffoldings commonly used in Italy and then proposed an

(a) (b) (c) (d) (e)

Figure 1: Pictures of different types of scaffolds. (a) Fastener scaffold. (b) Door-type scaffold. (c) Cuplock-type scaffold. (d) Access scaffold. (e) Inserting-type scaffold.

empirical formula to identify the critical load, which has certain reference significance on our research.

According to literature review and engineering investigation, failure of steel tubular scaffolds under uniform loads mainly occurs at the top 1-2 layers. Failure modes refer to the buckling of vertical rods or defection of top horizontal rods. Analysis of engineering accidents has revealed that the node joint instability is one of the major causes of scaffold collapse. The present study proposes two types of top-reinforced fastener steel tubular scaffold. To obtain a safe and stable structural form and scaffold system, a new steel tubular scaffold—mortise-and-tenon steel tubular scaffold—was developed with the Tianjin Xunan Jiahui Building Material Technology Co., Ltd. based on the concept of ancient wooden mortise-and-tenon joint structure [22]. Ultimate bearing capacities and failure modes of the reinforced fastening steel tubular scaffold and mortise-and-tenon steel tubular scaffold under uniform loads were studied through full-size experiments. Research conclusions provide technical support for engineering applications and standard specifications of tubular scaffolds.

2. Experiments

2.1. Design of Specimens and Material Properties. According to common construction scaffold structures, five experimental models were designed with comprehensive considerations to scaffold height, vertical and horizontal rod spaces, step distance of rods, height of bottom reinforcing rods, node connection modes, setting of vertical diagonal bracing, and processing methods of top horizontal steel rods. These models are shown in Table 1 and Figures 2–4. The 1–5 experimental models are (1) fastener steel tubular full-hall scaffold; (2) fastener steel tubular full-hall scaffold reinforced with top truss; (3) fastener steel tubular full-hall scaffold reinforced with top weak truss; (4) mortise-and-tenon steel tubular full-hall scaffold without diagonal bracing; and (5) mortise-and-tenon steel tubular full-hall scaffold with diagonal bracing.

In test samples, steel tubes were made out of Q235 with a nominal yield strength (f_y) of 235 MPa. The tensile coupons were cut from the same base metal of the steel tubes. Each group had three specimen samples with the same thickness, and the averaged data were collected, as shown in Table 2, where f_y is the yield strength, f_u is the ultimate tensile strength, δ is the percentage elongation after fracture, and E is the elastic modulus. The results verified that the steel material strength met the design requirements.

2.2. Loading Device. Figure 5 shows the loading device, which is mainly composed of counterforce frames, hydraulic jacks, box-type distribution beams, joist steels, and electric oil pumps. In the experiments, jacks that adopted parallel loading and eight hydraulic jacks with a range of 50 tons worked synchronously. The hydraulic jacks were divided into two groups and put on the vertical projection points at two box-type distribution beams of the counterforce frames. The 20a-type joist steels were paved uniformly on the horizontal rods that bore the top vertical stress in the loading range of the steel tubular scaffold. The box-type distribution beams had adequate rigidity, and sufficient joist steels were placed in a tight arrangement. Uniform linear loads were applied on top of the scaffold to simulate stress in actual engineering projects.

Table 1: Size of test models.

Project	Model 1	Model 2	Model 3	Model 4	Model 5
Height of scaffold (m)	5.60	5.60	5.60	5.16	5.16
Horizontal space between rods (m)	0.90	0.90	0.90	0.90	0.90
Vertical space between rods (m)	0.80~1.00	0.80~1.00	0.80~1.00	0.90	0.90
Step distance of rods (m)	1.35	1.35	1.35	1.20	1.20
Height of bottom horizontal rods (m)	0.2	0.2	0.2	0.36	0.36
Connection joint	Fastener joint	Fastener joint	Fastener joint	Mortise-and-tenon joint	Mortise-and-tenon joint
Diagonal bracing in surrounding regions	Yes	Yes	Yes	None	Yes
Top processing	None	Truss	Weak truss	None	None

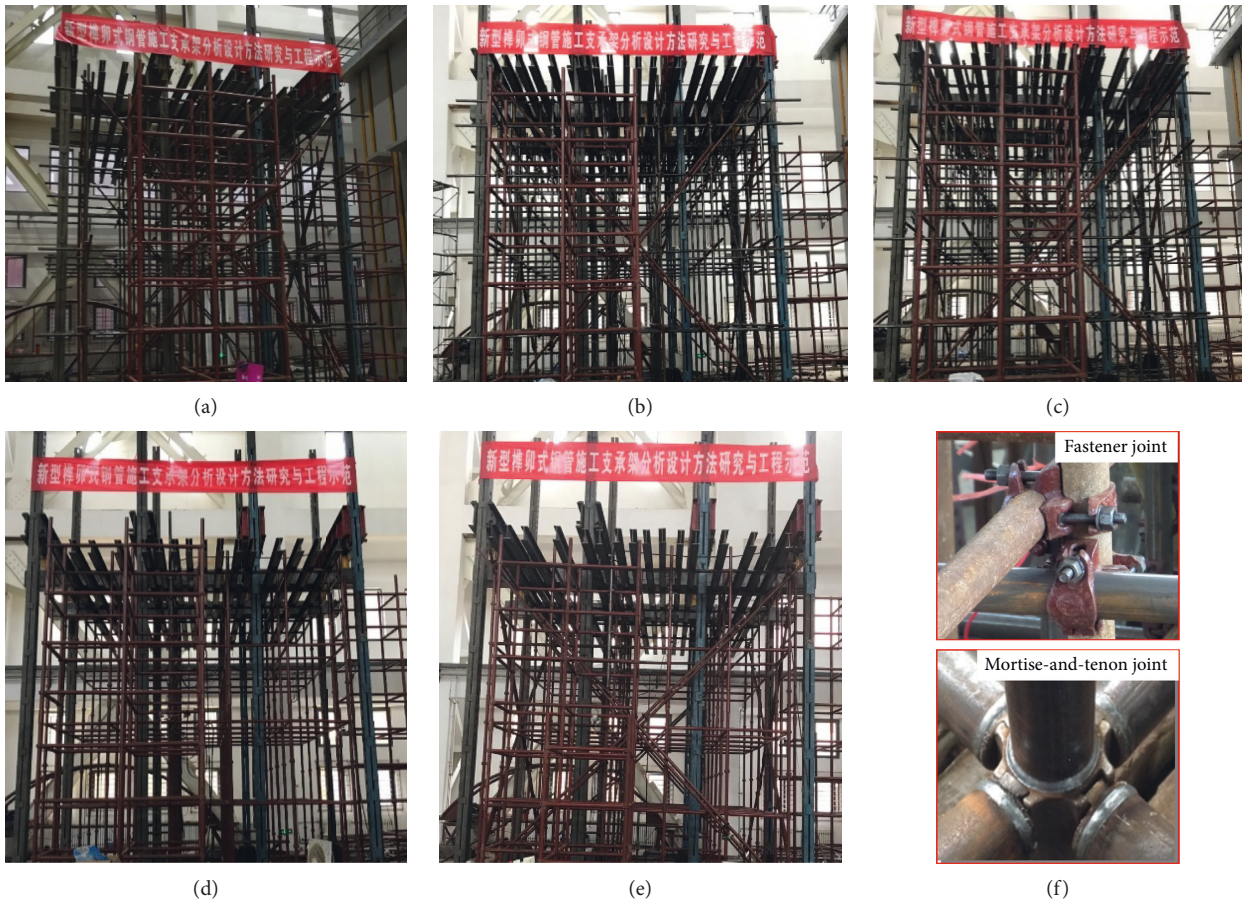

Figure 2: Overall structures of experimental models. (a) Fastener scaffold. (b) Fastener scaffold reinforced with truss. (c) Fastener scaffold reinforced with weak truss. (d) Mortise-and-tenon scaffold without diagonal bracing. (e) Mortise-and-tenon scaffold with diagonal bracing. (f) Types of joint.

2.3. Loading Systems. The loading process was divided into preloading, formal loading, and unloading.

Preloading was performed before formal loading. The preloading included two stages: 3 kN/rod and 6 kN/rod, to assure that the experiment proceeded smoothly. Formal loading was calculated according to loads of the whole frame. In the early stage, 300 kN was applied at each load increment and kept for 3 min. When the frame developed evident deformation, 150 kN was applied at each load increment and kept for 5 min. Approaching the ultimate bearing capacity of the frame, 75 kN was applied at each load increment and kept for at least 5 min. Succeeding loading stages continued until strain and displacement developed. The loading ended at frame failure, after which the load was kept for 10–15 min. Upon full-frame deformation, data and image were recollected and unloading followed in two stages. The loading system is shown in Table 3.

2.4. Layout of Measuring Points

2.4.1. Layout of Displacement Sensors. Six displacement sensors were arranged on the model to test out-of-plane displacement at upper, middle, and lower positions of the A-3 and C-6 rods. Sensors on the A-3 rod measured the

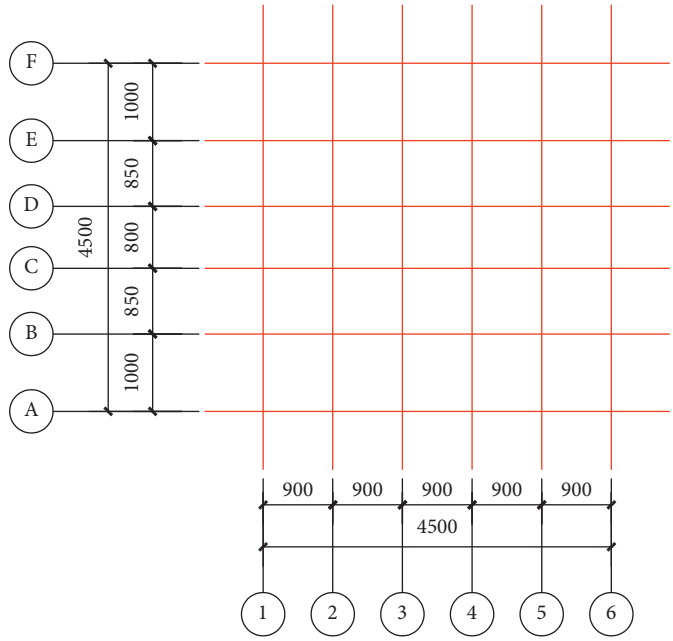

(a)

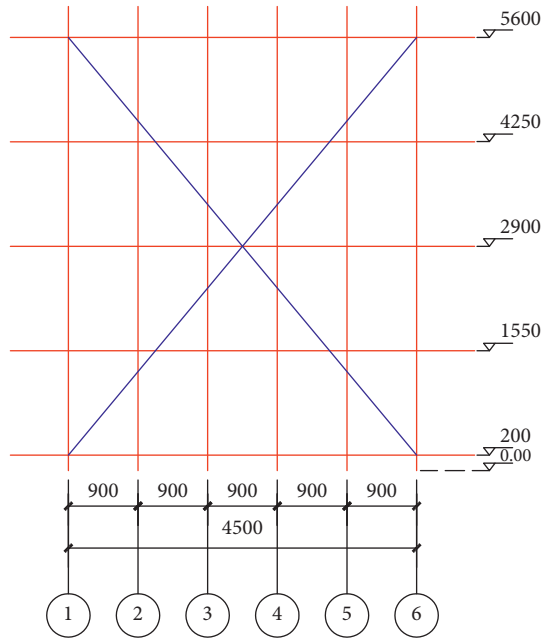

(b)

Figure 3: Continued.

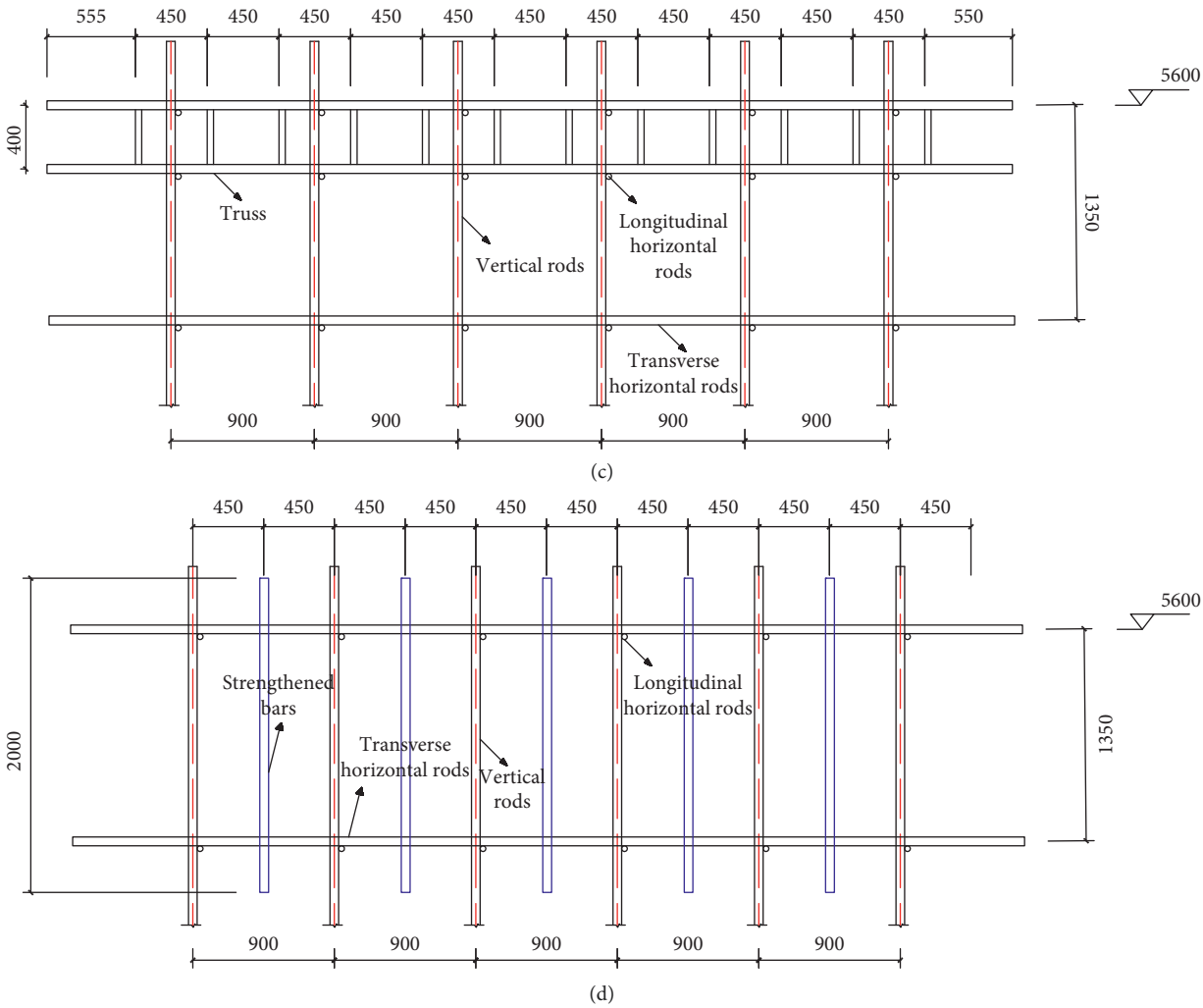

Figure 3: Structural layouts of Models 1, 2, and 3. (a) Plane view. (b) Vertical view. (c) Local view of the top of Model 2. (d) Local view of the top of Model 3.

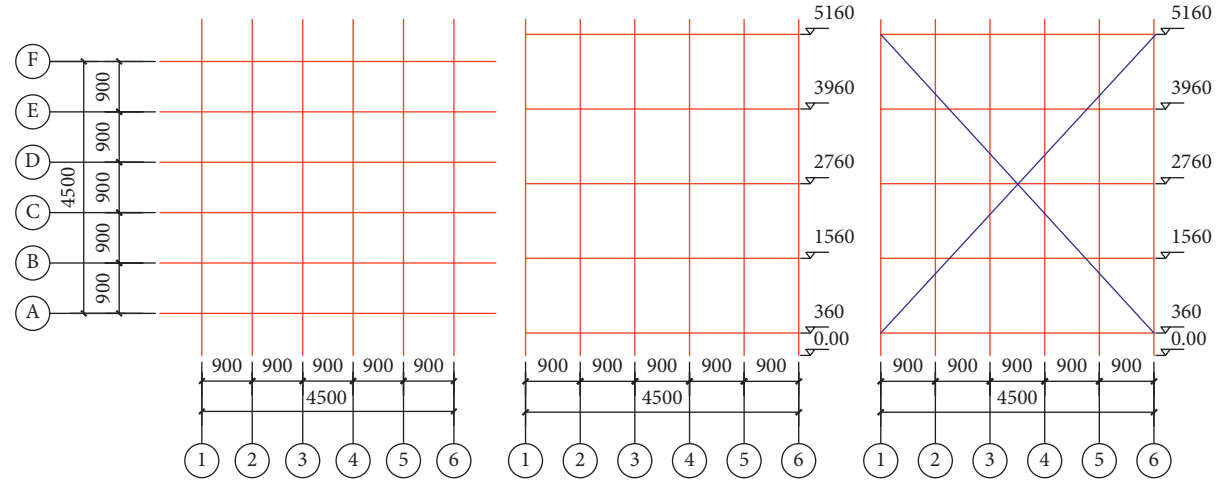

Figure 4: Structural layouts of Models 4 and 5. (a) Plane view. (b) Vertical view of Model 4. (c) Vertical view of Model 5.

Table 2: Test data of material properties.

Type	Diameter (mm)	Thickness (mm)	f_y (MPa)	f_u (MPa)	δ (%)	E (N/mm^2)
Steel tube	48.3	3	355	401	42	219000

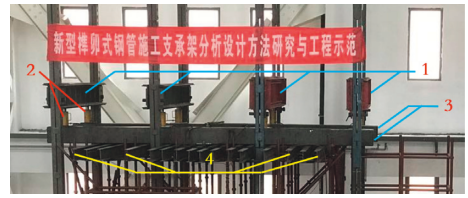

Figure 5: Loading device. (1) Counterforce frames; (2) hydraulic jacks; (3) box-type distribution beams; (4) 20a-type joist steels.

Table 3: Loading system in different experimental models.

Loading increment	1 (kN)	2 (kN)	3 (kN)	4 (kN)	5 (kN)	6 (kN)	7 (kN)	8 (kN)	9 (kN)
Model 1	300	450	600	750	825	900	—	—	—
Model 2	300	600	750	900	1050	1200	1350	1500	1575
Model 3	300	600	750	900	1050	1200	1350	1425	—
Model 4	300	600	750	900	975	1050	1125	—	—
Model 5	300	600	750	900	1050	1125	1140	1170	1200

north-south displacement and sensors on the C-6 rod measured the east-west displacement. Figures 6 and 7 show the layout of measuring points.

2.4.2. Layout of Strain Gauges. Loads on the fastening steel tubular full-hall scaffold were transmitted onto the ground through vertical rods. The top horizontal beam was the component that directly bears the stress of the scaffold. Bearing capacity of vertical rods and local buckling of horizontal rods could significantly influence the bearing capacity of the whole scaffold. Therefore, four strain gauges were placed symmetrically at each elevation of the three A-3 and C-6 rods. One strain gauge was placed at the middle of each span at the bottom of the A-axis and C-axis horizontal rods. Therefore, 34 strain gauges were placed on each model. Figures 8 and 9 show the layout of strain gauges on the vertical rods. Figures 10–13 show the layout of strain gauges on horizontal rods.

3. Experimental Phenomenon

3.1. Fastening Steel Tubular Full-Hall Scaffold. Fasteners emitted a light slippage sound when the load was increased from 450 kN to 600 kN. The top horizontal rods developed a slight down-deflection when the load was increased to 750 kN. A loud fastener slippage sound was heard when the loading was 705 kN. The load was increased to 875 kN, but it was immediately reduced to 840 kN due to failure of one fastener. The load was then gradually increased to 880 kN, when the west diagonal bracing and the rotary coupler that connects vertical rods failed. The load was dropped to 700 kN, ending the process. The buckling deformation of this specimen's vertical rods at failure was small. Evident large wave deflection was developed on the horizontal rods at the top, with a maximum deformation of 50 mm. A few top fasteners broke. The maximum slippage of top fasteners was 43.5 mm, which was observed at the top of C2. The failure situations are shown in Figure 14.

3.2. Fastening Steel Tubular Full-Hall Scaffold Reinforced with Top Truss. Fasteners emitted a light slippage sound when the load was increased from 1200 kN to 1350 kN, and a slight bending of vertical rods was observed. In the subsequent loading to 1500 kN, a loud fastener slippage sound was heard, and bending of vertical rods was observed. The load was increased to 1575 kN, and the overall bending deformation continued to increase. A small load reduction occurred when the load was maintained at 1575 kN through load supplementation. In this process, the entire vertical rods developed evident large wave buckling deformation (Figure 15(a)). The load was reduced to 1270 kN due to the breakage of one fastener, ending the process. The scaffold generally developed buckling failure. The horizontal rods of top truss developed evident flexural deflection (Figure 15(b)), and a fastener broke (Figure 15(c)). The maximum slippage of the top fastener was 25 mm, which was observed at the top of B5.

3.3. Fastening Steel Tubular Full-Hall Scaffold Reinforced with Top Weak Truss. Fasteners emitted a slippage sound when the load was increased from 900 kN to 1050 kN, but the vertical rods showed no significant deformation. The slippage sound became louder when the load was increased to 1200 kN, and flexural deflection of top horizontal rods was observed. The deformation sound became louder as the load was increased to 1350 kN, whereas some vertical rods developed bending deformation. In the subsequent loading to

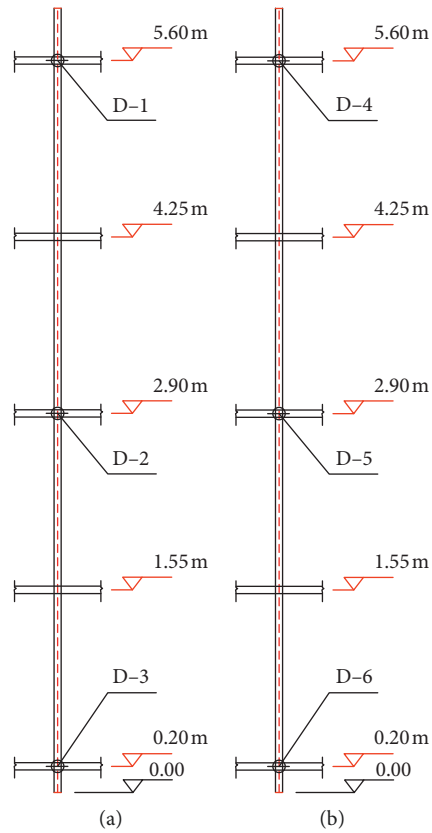

Figure 6: Layout of displacement sensors in Models 1, 2, and 3. (a) A-3 rod. (b) C-6 rod.

1425 kN, the flexural deformation of top horizontal rods increased and the buckling deformation of vertical rods became evident. The load was reduced while maintaining it at 1425 kN, supplemented upon reduction, and finally stabilized. The loading process ended. The overall deformation and buckling deformation of top horizontal rods are shown in Figure 16. The maximum slippage of top fasteners was 19 mm, which was observed at the top of F4.

3.4. Mortise-and-Tenon Steel Tubular Full-Hall Scaffold without Diagonal Bracing. The top horizontal rods bent slightly, but the vertical rods showed no significant deformation when the load was increased from 750 kN to 900 kN. The horizontal rods at the top slipped downward in the subsequent loading to 975 kN. Continuous slippage sounds were heard when the load was increased to 1050 kN, while slippage of top horizontal rods continuously increased. As the load increased to 1125 kN, the bending deformation of vertical rods similarly increased. The load was reduced while maintaining it at 1125 kN, which was compensated immediately to stabilize and end the loading process. In this model, the vertical rods developed concave deformation toward the west, while the top horizontal rods significantly slipped downward and showed local buckling. Some joints were disconnected and others showed compressive failure. The failure situations are shown in Figure 17. The maximum slippage of the tenon of the top mortise-and-tenon joint was 15 mm.

3.5. Mortise-and-Tenon Steel Tubular Full-Hall Scaffold with Diagonal Bracing. When the load was increased from 750 kN to 900 kN, the top horizontal rods bent slightly. A loud slippage sound was heard in the subsequent loading to 1125 kN. As the load increased to 1140 kN, the bending deformation of top horizontal rods increased and the vertical rods bent slightly. The slippage and bending deformation of top horizontal rods intensified at a load of 1170 kN. The load was reduced when it was maintained at 1200 kN, compensated immediately to stabilize. Finally, the loading process ended. In this model, the vertical rods developed small heave deformation, while the top horizontal rods significantly slipped downward. The joints showed local bending, compressive failure, and a few disconnections. The failure situations are shown in Figure 18. The maximum slippage of the tenon at the top mortise-and-tenon joint was 25 mm.

3.6. Bearing Capacity and Failure Mode. The ultimate bearing capacities and failure modes of five scaffold models are listed in Table 4. The bearing capacity of a single vertical rod in Model 2 was 43.75 kN, which was 87.5% higher than that in Model 1, indicating that using small truss reinforcement at the top could significantly increase the scaffold's material utilization. The bearing capacity of a single vertical rod in Model 3 was 39.6 kN, which was 69.9% higher than that in Model 1, indicating that this improvement could similarly increase material utilization. The bearing capacity of a single vertical rod in Model 3 was 9.4%

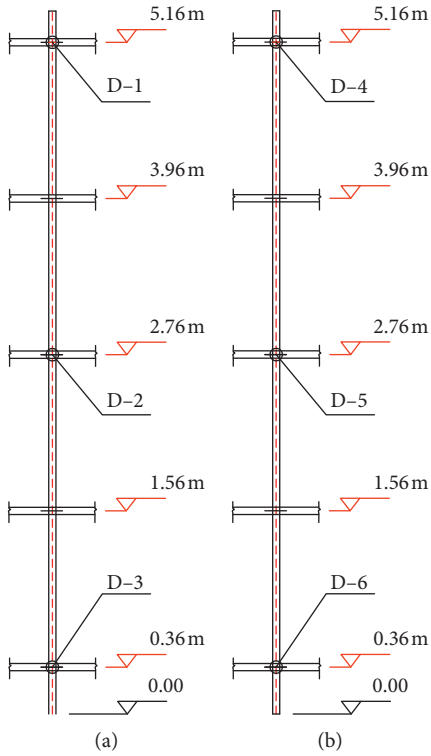

Figure 7: Layout of displacement sensors in Models 4 and 5. (a) A-3 rod. (b) C-6 rod.

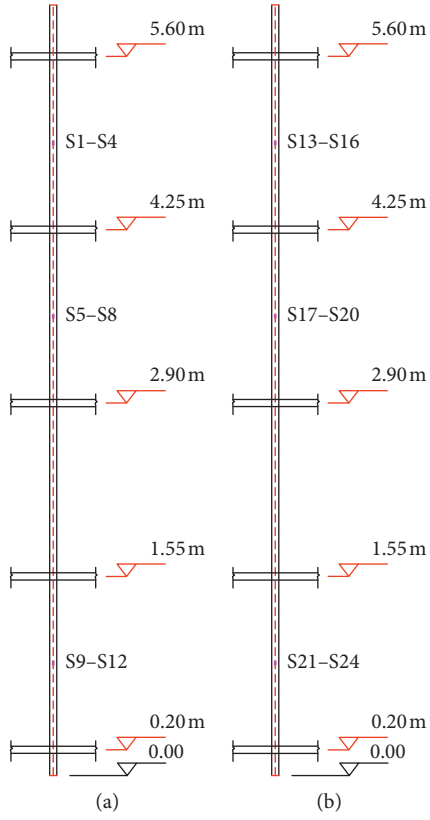

Figure 8: Layout of strain gauges on vertical rods of Models 1, 2, and 3. (a) A-3 rod. (b) C-6 rod.

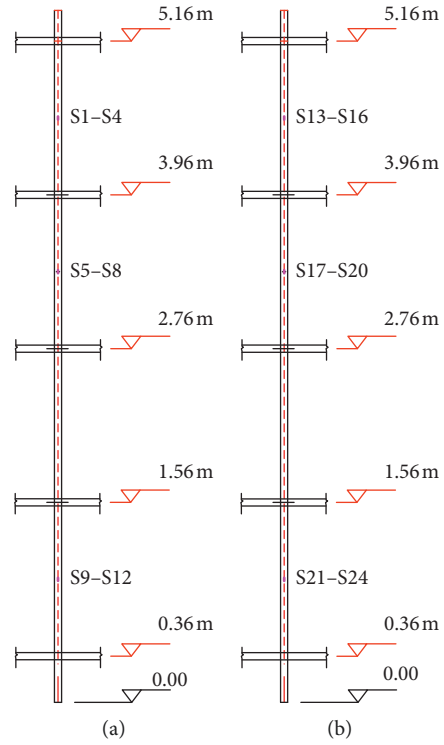

Figure 9: Layout of strain gauges on vertical rods of Models 4 and 5. (a) A-3 rod. (b) C-6 rod.

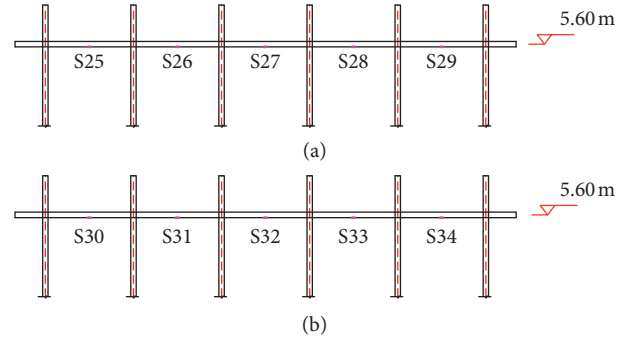

Figure 10: Layout of strain gauges on horizontal rods in Model 1. (a) A-axis horizontal beam. (b) C-axis horizontal beam.

lower than that in Model 2, showing a small reduction. The ultimate bearing capacity in Model 5 was 6.7% higher than that in Model 4, indicating that the vertical diagonal bracing influenced the ultimate bearing capacity of the mortise-and-tenon scaffold slightly. However, the diagonal bracing could constrain the deformation of vertical rods, and the failure mode changed from overall failure to local buckling of top horizontal rods.

4. Data Analysis of Measuring Points

4.1. Load-Displacement Data Analysis. Out-of-plane displacements from south to north at upper, middle, and lower positions of A-3 rods were collected by D1, D2, and D3. The

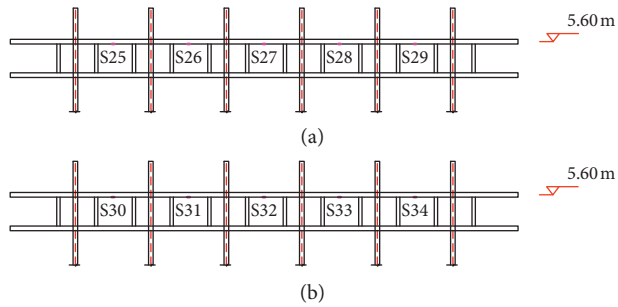

Figure 11: Layout of strain gauges on horizontal rods in Model 2. (a) A-axis horizontal beam. (b) C-axis horizontal beam.

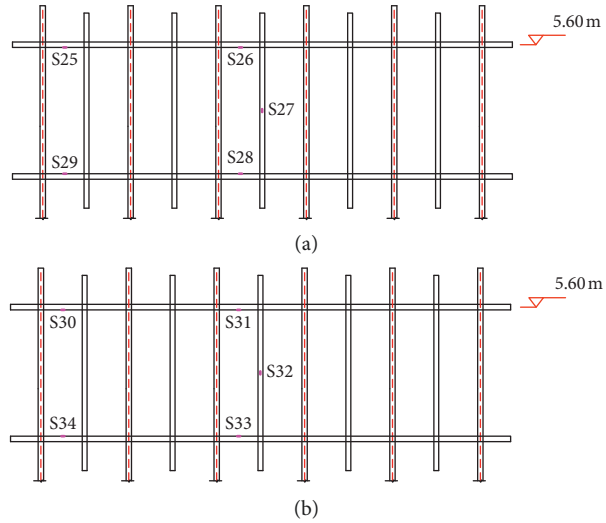

Figure 12: Layout of strain gauges on horizontal rods in Model 3. (a) A-axis horizontal beam. (b) C-axis horizontal beam.

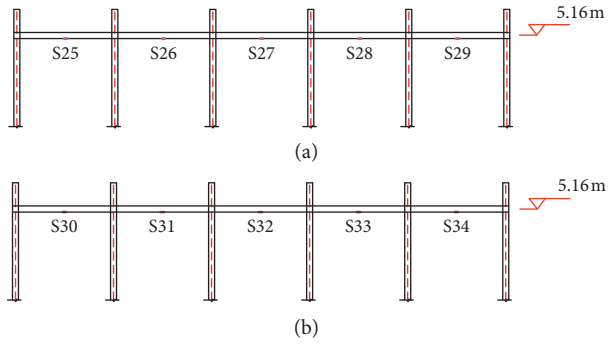

Figure 13: Layout of strain gauges on horizontal rods in Models 4 and 5. (a) A-axis horizontal beam. (b) C-axis horizontal beam.

out-of-plane displacements from east to west at upper, middle, and lower positions of C-6 rods were collected by D4, D5, and D6. The load-displacement curves of five experimental models are shown in Figures 18–22. On the whole, the vertical rods in the middle position of different experimental models showed a larger out-of-plane displacement compared with those at upper and lower positions. Figure 19 clearly shows that the general out-of-plane displacement of vertical rods in Model 1 was small and had no overall instability. Figure 20 shows that the out-of-plane displacement in Model 2 can reach a maximum of 30 mm, indicating serious overall instability. Figure 21 shows that the out-of-plane displacement at different elevations in Model 3 could be well coordinated and was smaller than that in Model 2, conforming to the experimental results of local buckling of vertical rods and weak overall instability. In Figure 22, the out-of-plane displacement of vertical rods in Model 4 could reach 30 mm. The maximum displacement at the middle of the vertical rod indicates serious overall instability. Figure 23 showed that the displacement results of Model 5 were similar to those of Model 3. The out-of-plane displacement of vertical rods at different elevations

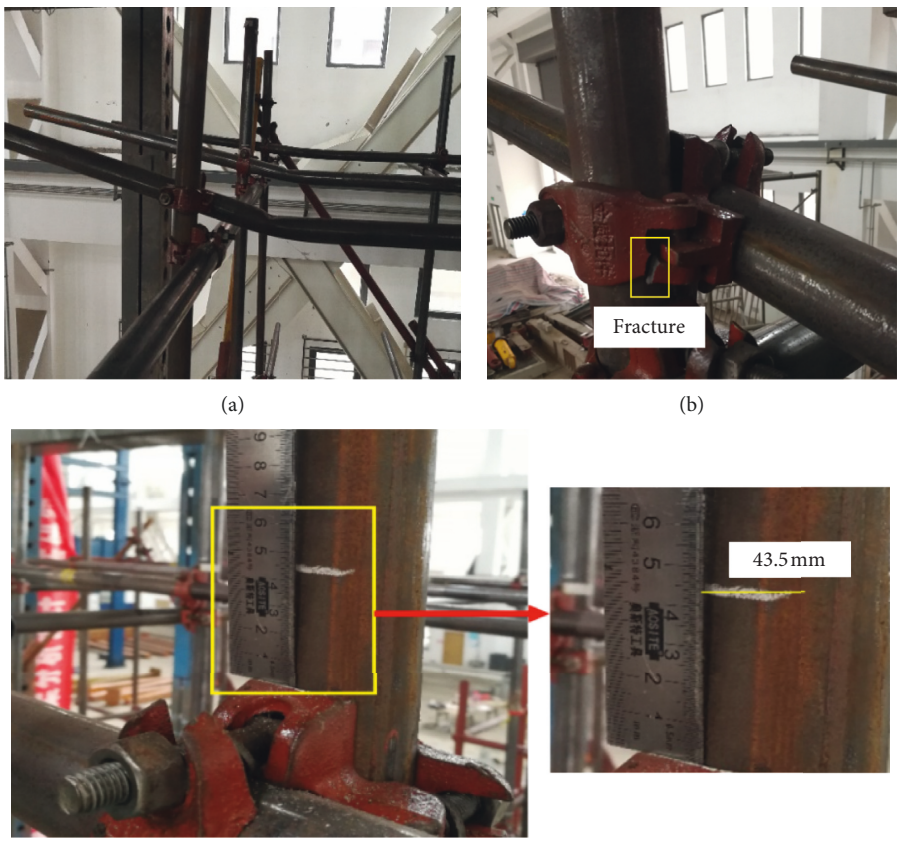

(a) (b) (c)

Figure 14: Failure situations of Model 1. (a) Deformation of horizontal rods. (b) Failure of top fasteners. (c) Slippage of fasteners.

(a) (b)

Figure 15: Failure situations of Model 2. (a) Overall buckling deformation of scaffold. (b) Bending of truss in the loading region. (c) Fastener failure at top of diagonal bracing.

(a)

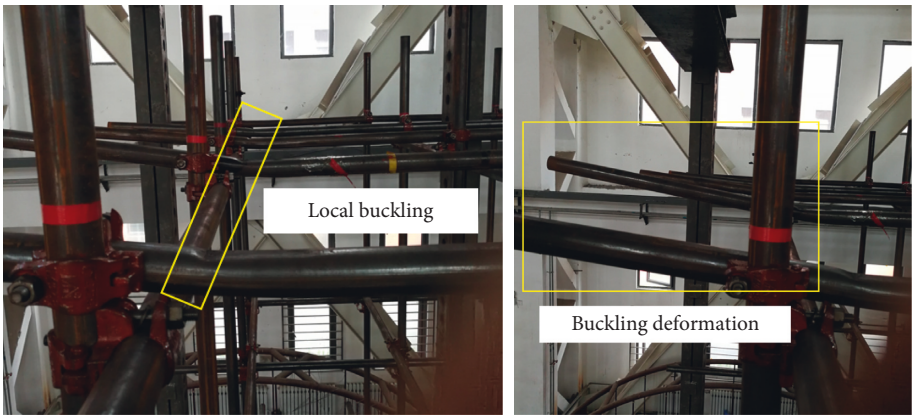

(b)

Figure 16: Failure situations of Model 3. (a) Overall buckling deformation of the scaffold. (b) Deformation of horizontal rods in the loading area.

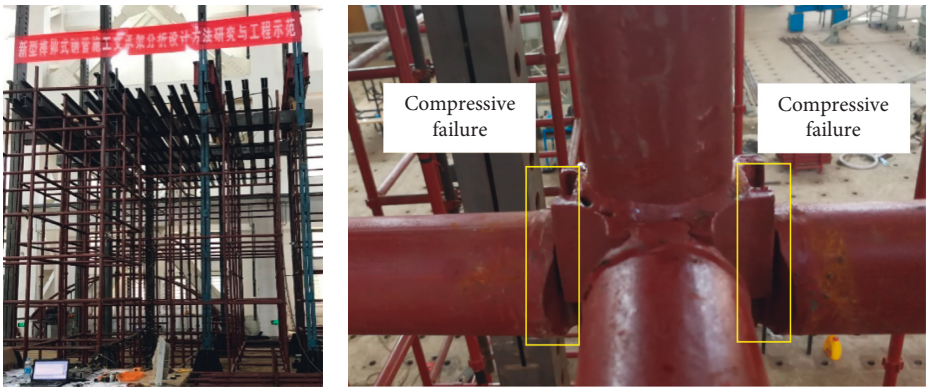

(a) (b)

Figure 17: Continued.

(c)

Figure 17: Failure situations of Model 4. (a) Overall buckling deformation of scaffold. (b) Failure of the top fastener. (c) Deformation of horizontal rods in the loading area.

(a) (b)

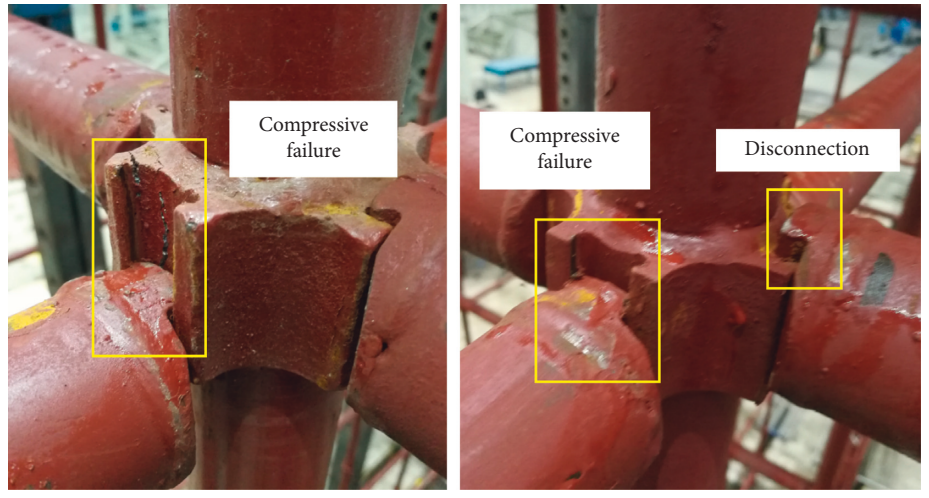

(c)

Figure 18: Failure situations of Model 5. (a) Overall buckling deformation of the scaffold. (b) Deformation of horizontal rods in the loading area. (c) Failure of a top fastener.

developed uniformly, and the diagonal bracing could effectively relieve overall instability.

4.2. Contrastive Analysis of Strain Data. The load-strain curves at positions with the maximum strain of the same vertical rod in Models 1, 2, and 3 are compared in Figure 24. The three models showed similar deformation trends of vertical rods during the loading process. Internal measuring points of vertical rods were mainly compressed, and the peripheral vertical rods might be locally stretched. The strain differences among the upper, middle, and lower positions of the vertical rod were small and loads were transmitted stably along the single vertical rod. The strain at measuring points suddenly increased in the late loading stage, followed by bending failure of the vertical rod. At model failure, strain at different positions of the vertical rod in Models 2 and 3 was approximately 1.5 times higher

Table 4: Summary of bearing capacity and failure modes of experimental models.

Models	Overall ultimate bearing capacity (kN)	Ultimate bearing capacity of single vertical rod (kN)	Main failure modes	Maximum slippage of joints (mm)
1	840	23.3	Defection of top horizontal rods and breakage of fasteners	43.5
2	1575	43.75	Overall instability	25
3	1425	39.6	Deflection of top horizontal rods and local buckling of vertical rods	19
4	1125	31.25	Overall instability, local buckling of top horizontal rods, compressive joint failure, and disconnection of several joints	15
5	1200	33.3	Local buckling of top horizontal rods and compressive joint failure	25

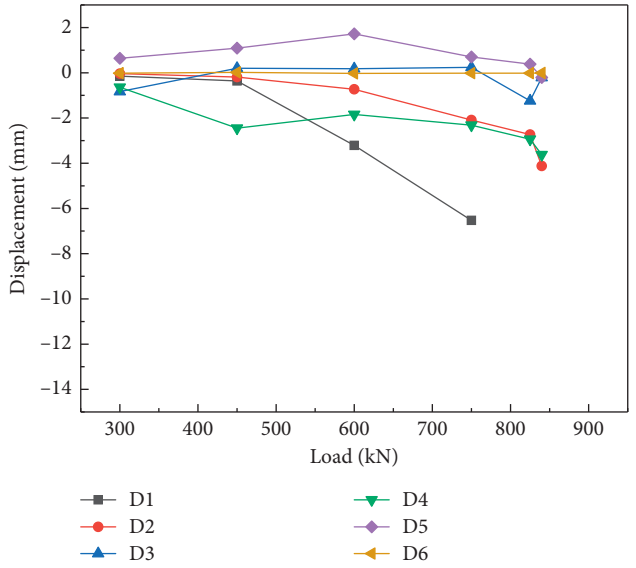

Figure 19: Load-displacement curves in Model 1.

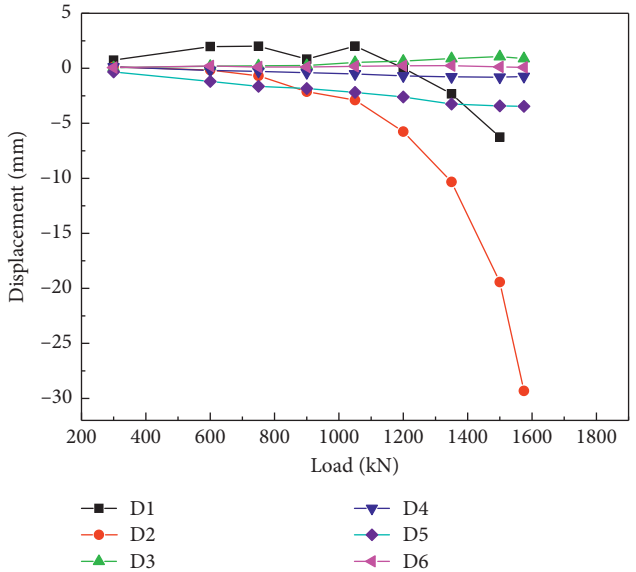

Figure 20: Load-displacement curves in Model 2.

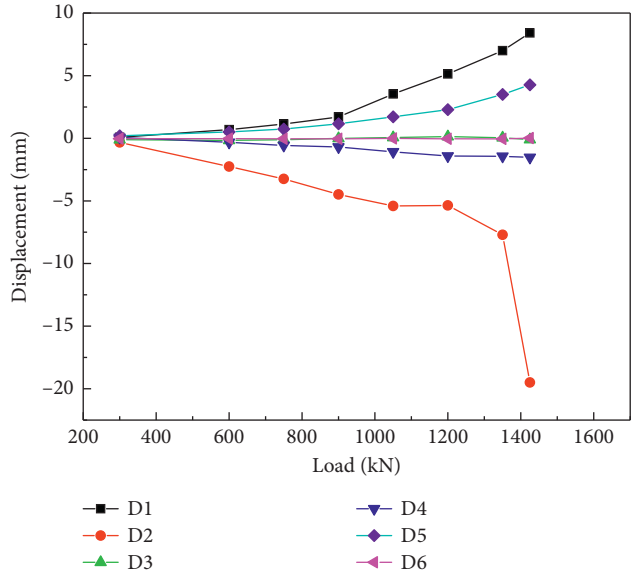

Figure 21: Load-displacement curves in Model 3.

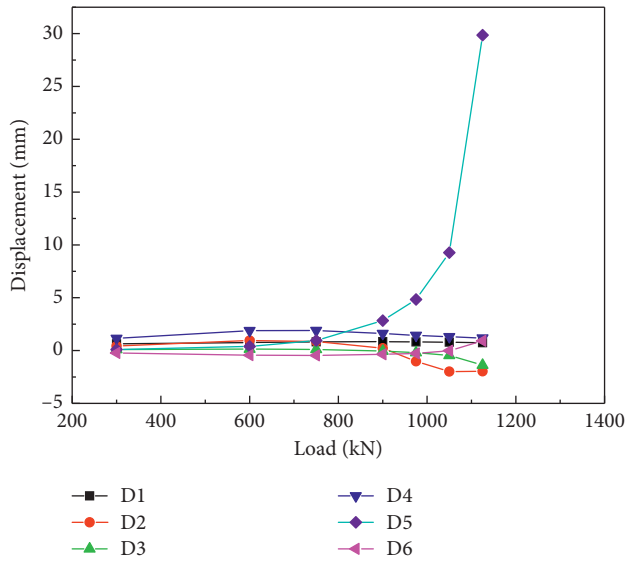

Figure 22: Load-displacement curves in Model 4.

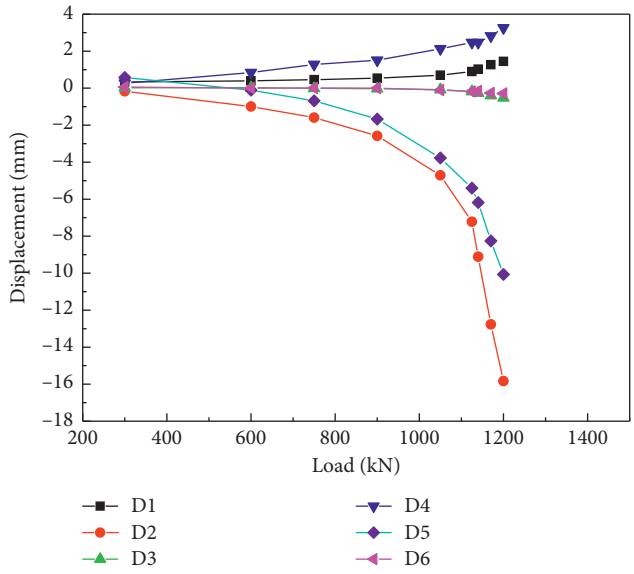

Figure 23: Load-displacement curves in Model 5.

compared with that in Model 1. The strain in Models 1 and 2 was similar.

Comparisons of strain of horizontal rods in Models 1 and 2 are shown in Figure 25. Failure of these two models showed similar deformation trends at different positions. The bearing capacity and deformation ability of Model 2 significantly increased. Overall instability was the major failure mode in Model 2. Deformations of the vertical and horizontal rods were more coordinated and the bearing capacity of vertical rods developed more thoroughly. The fastener steel tubular full-hall scaffold reinforced with top truss proved to be more cost-effective and safer.

The load-strain curves at A-axis and C-axis horizontal rods in Models 1, 2, and 3 are compared in Figure 26. The horizontal rods of all three models developed larger sidespan than midspan deformation, and sidespan yielding came earlier than midspan yielding. In Models 1 and 2, the deformation of C-axis horizontal rods was significantly larger than that of A-axis horizontal rods. The deformation of A-axis and C-axis horizontal beams in Model 3 was similar, indicating that the deformation of top axial horizontal rods in the fastening steel tubular full-hall scaffold reinforced with top weak truss was more coordinated.

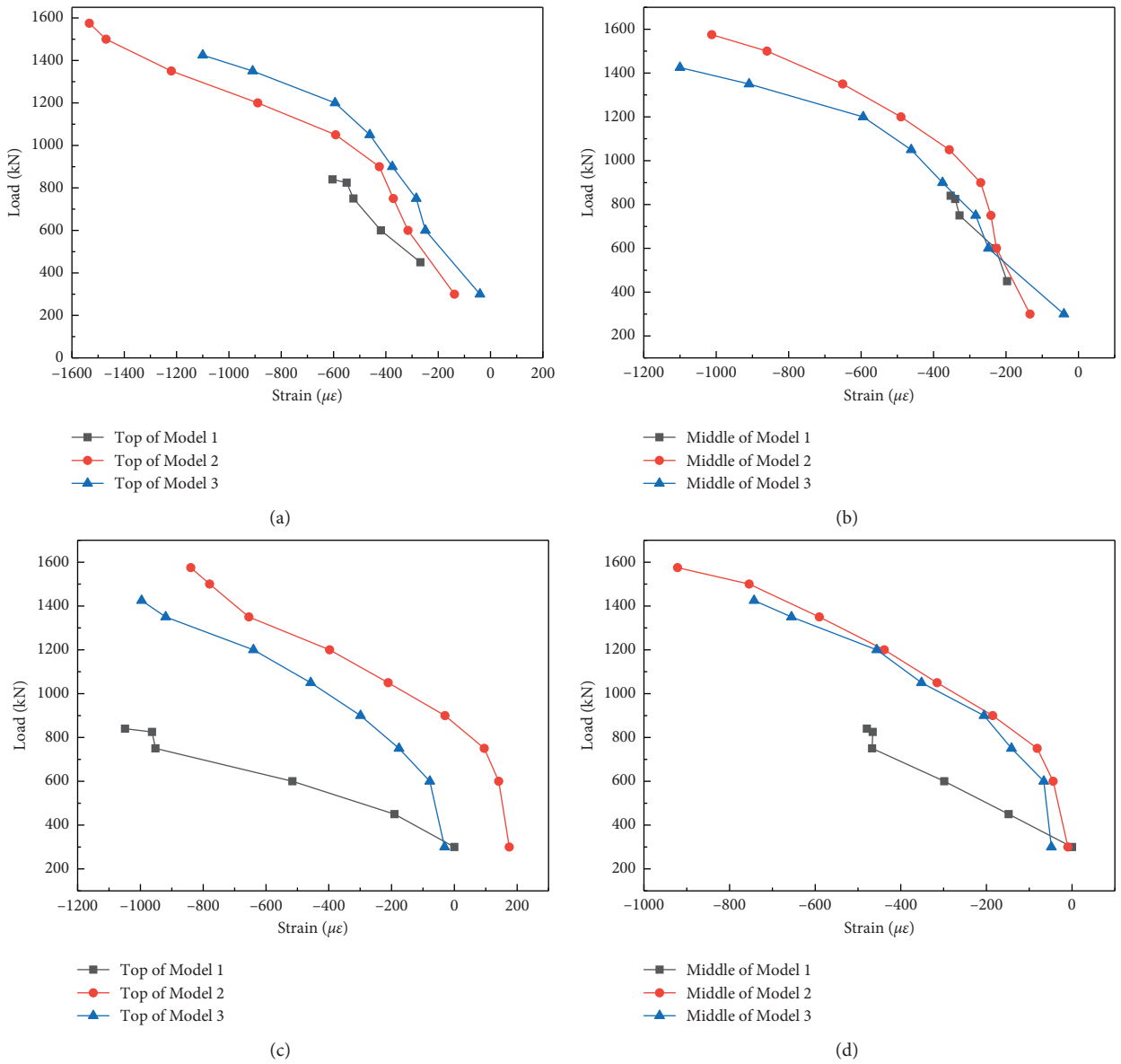

Figure 24: Comparison of load-strain curves of vertical rod in Models 1, 2, and 3. (a) Top of A3 rod. (b) Middle of A3 rod. (c) Top of C3 rod. (d) Middle of C3 rod.

Clearly, the improved fastener steel tubular scaffold reinforced with top weak truss increased the material utilization to some extent. However, its improvement on the bearing capacity of top horizontal rods is less than that of the fastener steel tubular scaffold reinforced with top truss. Therefore, deflection of top horizontal rods was the main failure mode and the structural integrity was lower than that of the fastening steel tubular scaffold reinforced with top truss.

The load-strain curves at measuring points with the maximum strain in Models 1 and 4 are compared in Figure 27. The mortise-and-tenon steel tubular full-hall scaffold without diagonal bracing showed similar load-strain curves but higher bearing capacity, when compared with those of the fastener steel tubular full-hall scaffold. Thus, given the same loads, the mortise-and-tenon scaffold showed smaller strain and stronger stability.

The load-strain curves at the measuring points with maximum strain of vertical rods in Models 4 and 5 are compared in Figure 28. The two scaffolds show similar load-strain curves. The strain at upper, middle, and lower positions of the vertical rods was similar and loads were transmitted stably along single vertical rods. In the late loading stage, the strain at measuring points suddenly increased, followed by bending failure of the vertical rods. Bearing capacities and strain were likewise similar between the two scaffolds, indicating that the vertical diagonal bracing could constrain vertical rods to change the overall failure into local bending of top horizontal rods.

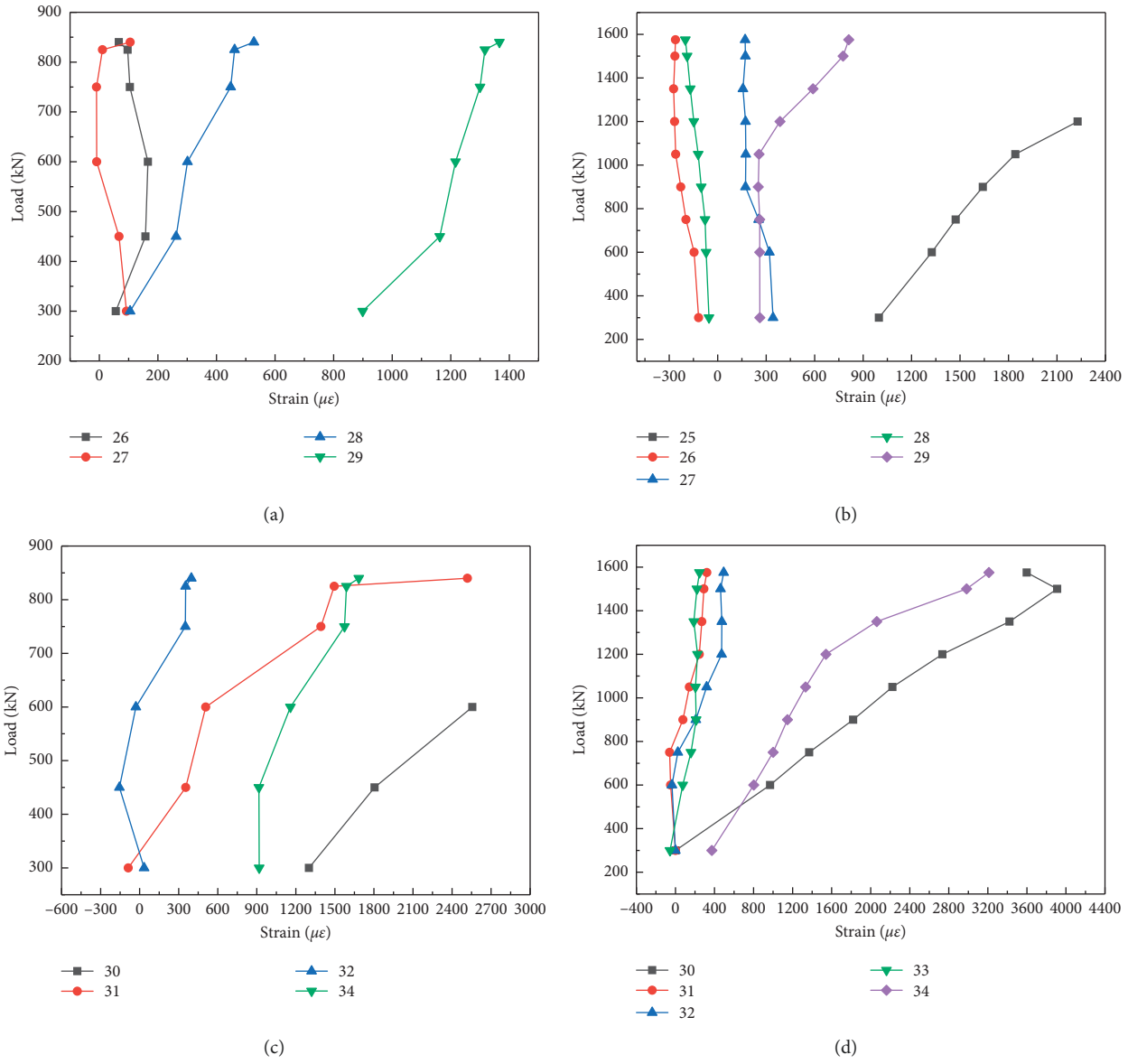

Figure 25: Comparison of load-strain curves of horizontal beams in Models 1 and 2. (a) A-axis horizontal rods of Model 1. (b) A-axis horizontal rods of Model 2. (c) C-axis horizontal rods of Model 1. (d) C-axis horizontal rods of Model 2.

However, the diagonal bracing failed to increase the bearing capacity.

4.3. Discussion and Suggestions. As we know, scaffolds have been widely applied in engineering construction. However, due to the inadequate design and the unknown overloads on site, the structural failure of the scaffoldings occurs, resulting in numerous worker injuries and property loss. In response to the above situation, two types of top-reinforced fastener steel tubular scaffold and mortise-and-tenon steel tubular scaffold were proposed through experiments. Compared with traditional scaffolding, their bearing capacity was greatly improved, which provided more alternative novel scaffolds to meet safety requirements. When the traditional scaffolding capacity was insufficient in engineering, it was suggested that the program with the reinforcement of top small truss in scaffolds could be adopted, which had a significant effect. In addition, the research conclusions could provide technical support for engineering applications and standard specifications of tubular scaffolds.

5. Conclusions

(1) The bearing capacity of single vertical rods in the fastener steel tubular scaffold reinforced with top truss is 43.75 kN, which is 87.5% higher than that in traditional fastening steel tubular scaffold. The reinforcement of top small truss can significantly increase the scaffold's material utilization.

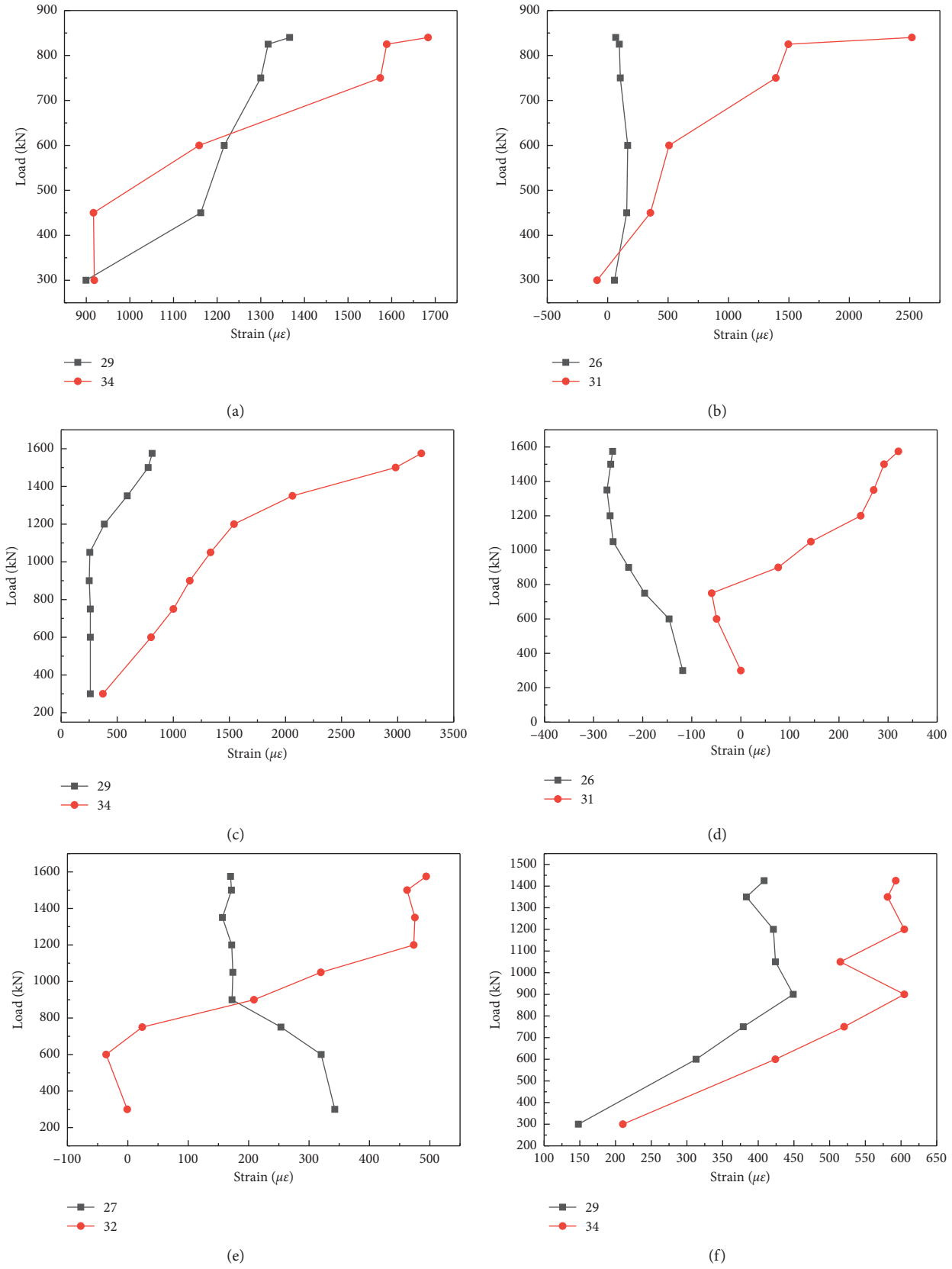

Figure 26: Continued.

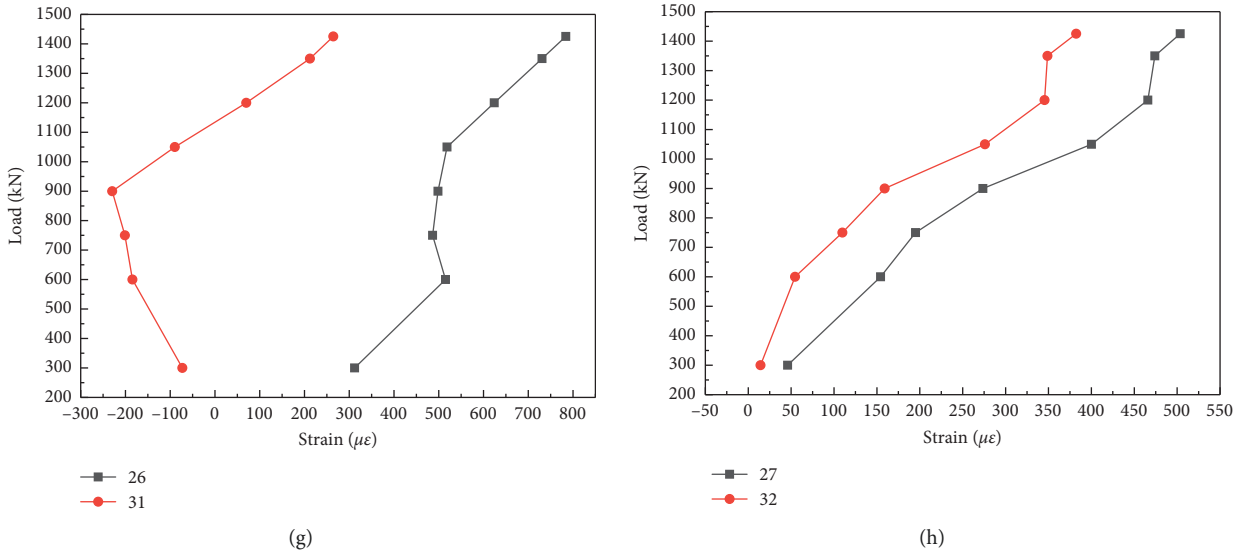

Figure 26: Load-strain curves of A-axis and C-axis horizontal rods in Models 1, 2, and 3. (a) The sidespan in Model 1. (b) The second span in Model 1. (c) The sidespan in Model 2. (d) The second span in Model 2. (e) The midspan in Model 2. (f) The sidespan in Model 3. (g) The second span in Model 3. (h) The midspan in Model 3.

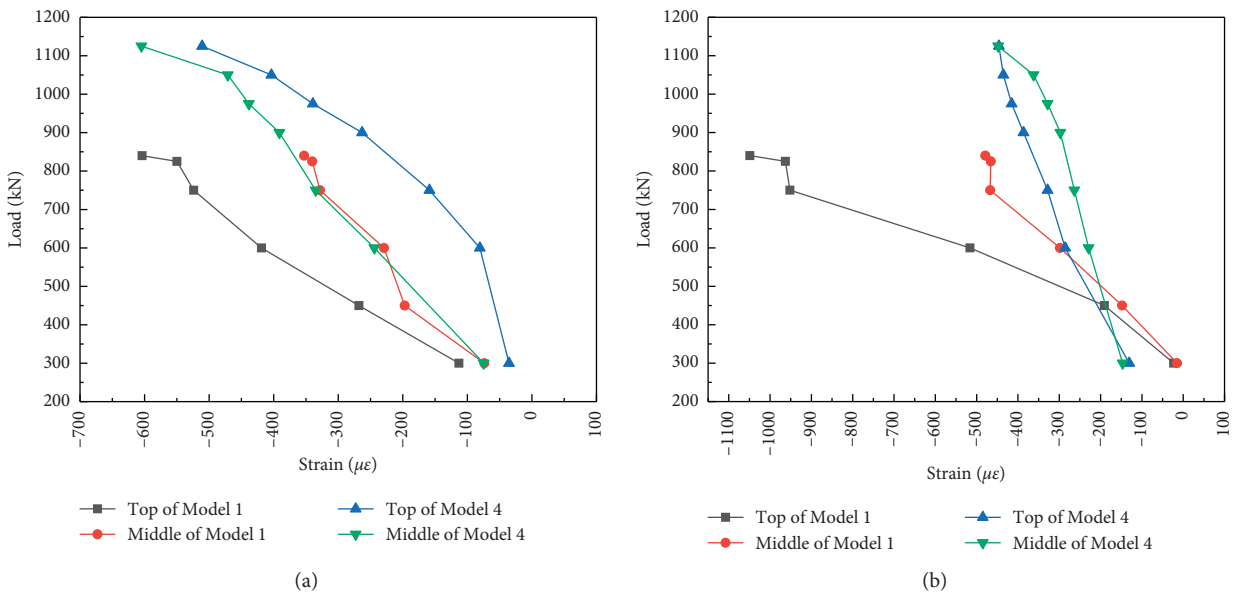

Figure 27: Load-strain curves of vertical rods in Models 1 and 4. (a) Comparison of A3 rod. (b) Comparison of C3 rod.

The maximum out-of-plane displacement reaches 30 mm, indicating serious overall buckling.

(2) The bearing capacity of the scaffold reinforced with top weak truss was 9.4% lower than that of scaffold reinforced with top truss. Compared with the scaffold reinforced with top truss, the scaffold reinforced with top weak truss shows poorer structural integrity, more coordinated deformation of top horizontal rods, and weaker overall instability. Deflection of top horizontal rods is the main failure mode.

(3) Loads on the mortise-and-tenon scaffold transmit stably along single vertical rods. The ultimate bearing capacity of Model 5 is 6.7% higher than that of Model 4, indicating that the vertical diagonal bracing slightly influences the ultimate bearing capacity. However, the vertical diagonal bracing can constrain the deformation of vertical rods, changing the failure mode of the mortise-and-tenon scaffold from overall failure to local buckling of top horizontal rods.

(4) The maximum slippage of the mortise-and-tenon scaffold is lower than that of the fastener scaffold, whereas its bearing capacity is higher. Given the same load, the mortise-and-tenon steel tubular full-hall scaffold shows smaller strain and stronger

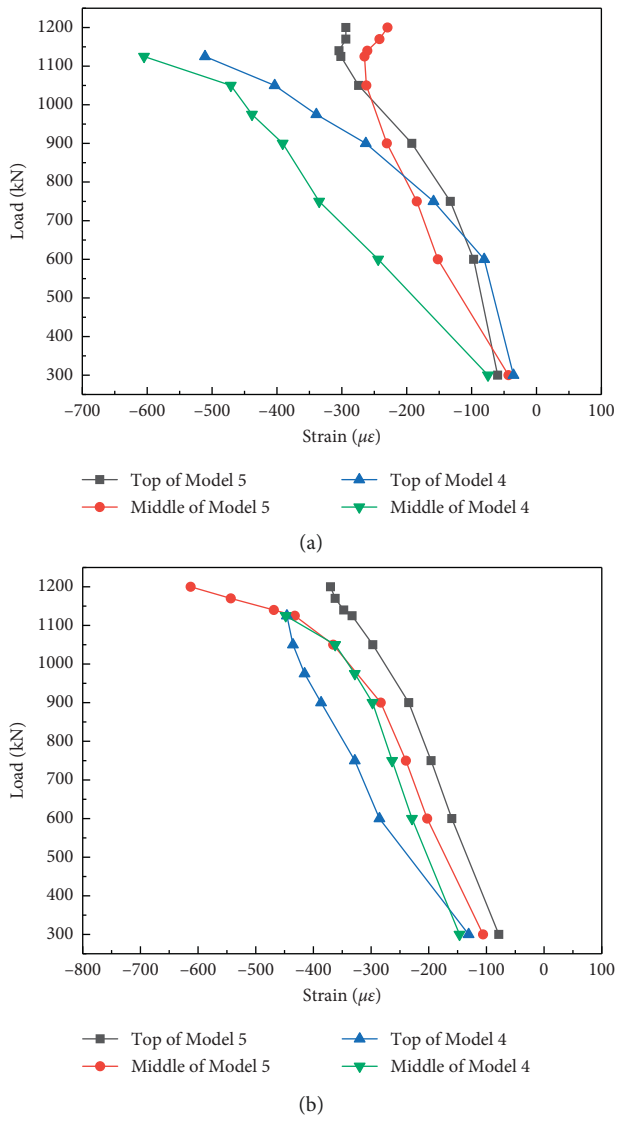

FIGURE 28: Load-strain curves of vertical rods in Models 4 and 5. (a) Comparison of A3 rod. (b) Comparison of C3 rod.

stability. However, reinforcement at top layers could offset the disadvantages of the fastener scaffold.

Data Availability

The data used to support the findings of this study are available from the first author and corresponding author upon request.

Conflicts of Interest

The authors declare that they have no conflicts of interest.

References

[1] S. L. Chan, Z. H. Zhou, W. F. Chen, J. L. Peng, and A. D. Pan, "Stability analysis of semirigid steel scaffolding," *Engineering Structures*, vol. 17, no. 8, pp. 568–574, 1995.

[2] J. L. Peng, A. D. Pan, D. V. Rosowsky, W. F. Chen, T. Yen, and S. L. Chan, "High clearance scaffold systems during construction -I. Structural modelling and modes of failure," *Engineering Structures*, vol. 18, no. 3, pp. 247–257, 1996.

[3] J. L. Peng, A. D. Pan, D. V. Rosowsky, W. F. Chen, T. Yen, and S. L. Chan, "High clearance scaffold systems during construction -II. Structural analysis and development of design guidelines," *Engineering Structures*, vol. 18, no. 3, pp. 258–267, 1996.

[4] J. L. Peng, A. D. E. Pan, W. F. Chen, T. Yen, and S. L. Chan, "Structural modeling and analysis of modular falsework systems," *Journal of Structural Engineering*, vol. 123, no. 9, pp. 1245–1251, 1997.

[5] J. L. Peng, A. D. E. Pan, and S. L. Chan, "Simplified models for analysis and design of modular falsework," *Journal of Constructional Steel Research*, vol. 48, no. 2-3, pp. 189–209, 1998.

[6] J. L. Peng, A. D. E. Pan, and W. F. Chen, "Approximate analysis method for modular tubular falsework," *Journal of Structural Engineering*, vol. 127, no. 3, pp. 256–263, 2001.

[7] L. B. Weesner and H. L. Jones, "Experimental and analytical capacity of frame scaffolding," *Engineering Structures*, vol. 23, no. 6, pp. 592–599, 2001.

[8] W. K. Yu, K. F. Chung, and S. L. Chan, "Structural instability of multi-storey door-type modular steel scaffolds," *Engineering Structures*, vol. 26, no. 7, pp. 867–881, 2004.

[9] M. Pienko and E. Blazik-Borowa, "Numerical analysis of load-bearing capacity of modular scaffolding nodes," *Engineering Structures*, vol. 48, pp. 1–9, 2013.

[10] J.-L. Peng, C.-W. Wu, S.-L. Chan, and C.-H. Huang, "Experimental and numerical studies of practical system scaffolds," *Journal of Constructional Steel Research*, vol. 91, pp. 64–75, 2013.

[11] H. Zhang, K. J. R. Rasmussen, and B. R. Ellingwood, "Reliability assessment of steel scaffold shoring structures for concrete formwork," *Engineering Structures*, vol. 36, pp. 81–89, 2012.

[12] H. Zhang and K. J. R. Rasmussen, "System-based design for steel scaffold structures using advanced analysis," *Journal of Constructional Steel Research*, vol. 89, pp. 1–8, 2013.

[13] H. Zhang, T. Chandrangsu, and K. J. R. Rasmussen, "Probabilistic study of the strength of steel scaffold systems," *Structural Safety*, vol. 32, no. 6, pp. 393–401, 2010.

[14] M. H. R. Godley and R. G. Beale, "Sway stiffness of scaffold structures," *The Structural Engineer*, vol. 75, no. 14, p. 224, 1997.

[15] R. G. Beale and M. H. R. Godley, "Numerical modelling of tube and fitting access scaffold systems," *Advanced Steel Construction*, vol. 2, no. 3, pp. 199–223, 2006.

[16] R. G. Beale, "Scaffold research—a review," *Journal of Constructional Steel Research*, vol. 98, pp. 188–200, 2014.

[17] F. Yue, Y. Yuan, G. Q. Li, K. M. Ye, Z. M. Chen, and Z. P. Wang, "Wind load on integral-lift scaffolds for tall building construction," *Journal of Structural Engineering*, vol. 131, no. 5, pp. 816–824, 2005.

[18] H. F. Ao and G. Q. Li, "Investigation of overall load-bearing stability capacity of tube-and-coupler scaffolds," *Chinese Quarterly of Mechanics*, vol. 25, pp. 213–218, 2004, in Chinese.

[19] H. Liu, Q. Zhao, X. Wang et al., "Experimental and analytical studies on the stability of structural steel tube and coupler scaffolds without X-bracing," *Engineering Structures*, vol. 32, no. 4, pp. 1003–1015, 2010.

[20] H. B. Liu, Z. H. Chen, X. D. Wang et al., "Theoretical analysis and experimental research on stability behavior of structural

steel tube and coupler falsework with X-bracing," *Advanced Steel Construction*, vol. 6, no. 4, pp. 946–962, 2010.

[21] G. P. Cimellaro and M. Domaneschi, "Stability analysis of different types of steel scaffolds," *Engineering Structures*, vol. 152, pp. 535–548, 2017.

[22] X. He, *Study of the Ultimate Bearing Capacity of Full-Hall Formwork Support System of Mortise and Tenon Joints*, Tianjin University, Tianjin, China, 2014, in Chinese.

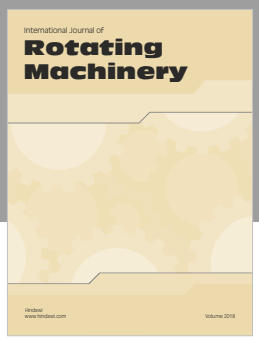

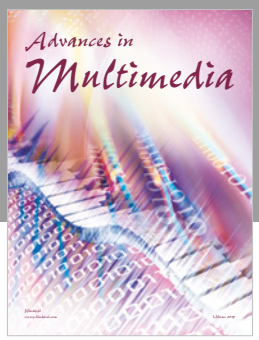

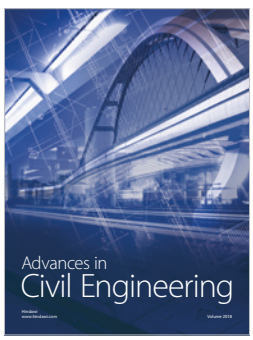

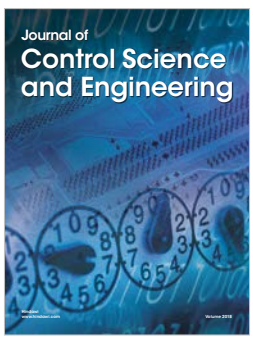

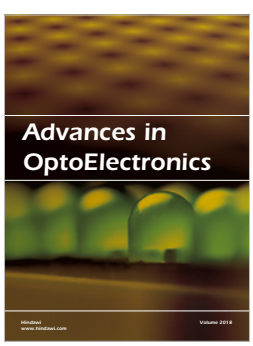

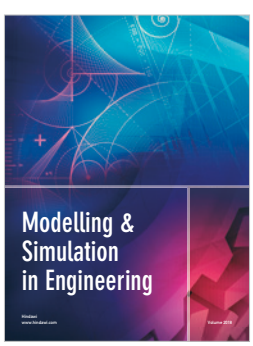

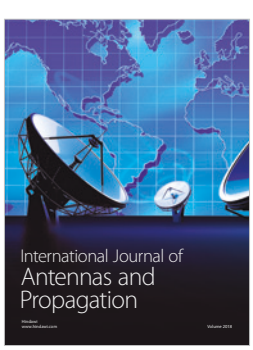

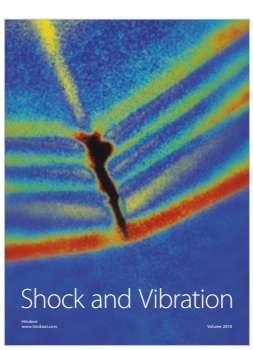

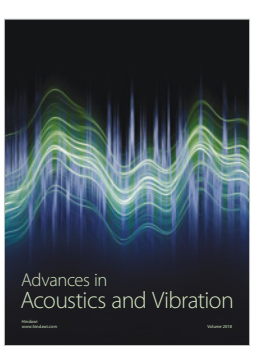

Hindawi

Submit your manuscripts at
www.hindawi.com